Lasers in Manufacturing Conference 2019

Thermo-Fluidic Modelling of Meltpool Instabilities during Laser Metal Deposition of Inconel 625

Akash Aggrawal[a*], A. R. Vinod[b] , Arvind Kumar[a]

[a]*Department of Mechanical Engineering, Indian Institute of Technology Kanpur, Kanpur - 208016, India*
[b]*Department of Ultra Precision Engineering, Central Manufacturing Technology Institute, Bengaluru- 560022, India*

Abstract

A three-dimensional particle scale heat transfer and fluid flow solver is developed in OpenFOAM to study the transport phenomena (convection, melting/ solidification phase change and ripples formation) in the Laser Metal Deposition (LMD) process. Getting precise information about the powder stream (particle size and distribution) in the LMD process is critical for the particle scale modelling. The current work uses a realistic powder stream insertion method. Once the powder stream information is obtained, the particle distribution is exported to an open source CFD code OpenFOAM. The Volume of Fluid method is used to identify and track the interface of the powder particles undergoing phase transition. The developed computational model helps to understand laser/matter interaction, melting of particles, the formation of the fusion zone, melt pool instabilities and ripples generation mechanism. The computational results were found consistent with the measured experimental data on melt pool dimensions.

Keywords: Laser metal deposition; OpenFOAM; Heat transfer and fluid flow; Ripple formation; Melt pool instabilities

1. Introduction

Laser metal deposition (LMD) process accompanies various physical phenomena such as beam - particle and beam-substrate interaction, impingement of molten particles with the molten pool creating oscillation on the free surface, mass and energy addition due to powder particles, , flow due to thermal gradient on the free surface (Marangoni convection) and also because of impinging powder particles (Lee et al., 2014 and Manvatkar et al., 2014). The sequential impingement of the powder particles in the melt pool creates instability leading to oscillating transport phenomena in LMD process. Although there are some work reported during the LMD process (Kumar et al., 2009 and Lee et al., 2016), but its formation mechanism and instability formation is not understood.

In this paper, a particle scale model is developed using open-source code OpenFOAM to study the melt pool dynamics in the SLM process. A a realistic powder stream insertion method is used to determine the deposition of the Inconel 625 particles in the substrate. Thereafter, the volume of fluid approach using

* Corresponding author. Tel.: +91-737-610-6811 ;
E-mail address: akashagg@iitk.ac.in .

the finite volume method is used to identify and track the interface of the powder particles undergoing phase transition. Subsequently, geometrical characteristics of the melt pool dimensions obtained by computational modelling are quantitatively validated with the in-house single spot experiments.

2. NUMERICAL MODELLING AND METHODOLOGY

To understand the interaction of high energy beam with the Inconel 625 powder particles and the substrate, single spot deposition over a substrate is simulated with the help of a thermo-fluidic particle scale model. The developed thermo-fluidic powder scale model uses a realistic powder stream for CFD modelling and incorporates the physics of laser irradiation on the substrate, particle impingement on the molten pool, melt flow due to thermo-capillary force and the phase transition. Firstly, a cloud of randomly generated particles was generated inside the computational domain. Thereafter, thermo-fluidic simulation was carried out using an open source CFD C++ code OpenFOAM.

Figure 1a shows the computational domain considered for the single spot deposition. The computational domain consists of an Inconel 625 substrate, an argon inert gas region and an Inconel 625 powder stream (Fig. 1b). In the model, transient heat transfer and fluid flow dynamics in the melt pool are considered using the volume of fluid surface tracking method (VOF). The VOF transport equation for interface tracking between two immiscible phases (Inconel 625 and argon gas) is given by

$$\frac{\partial \gamma}{\partial t} + \nabla \cdot \left(\gamma \vec{U}\right) + \nabla \cdot \left((1-\gamma)\gamma \overrightarrow{U_r}\right) = 0 \tag{1}$$

where γ is the phase fraction, $\vec{U}$ is the velocity vector and $\overrightarrow{U_r}$ is the compression velocity.
In the modelling, the thermo-physical properties of the two immiscible phases are calculated using the continuum formulation based on the classical mixture theory. Assuming the flow to be incompressible, laminar and Newtonian, the governing conservation equations for mass, momentum and energy conservation are formulated. The governing energy conservation equation is given by

$$\frac{\partial (\rho C_p T)}{\partial t} + \nabla \cdot \left(\rho \vec{U}\, C_p T\right) = \nabla \cdot (k \nabla T) + S_{Latent} + Q_{Losses} + Q_{Laser} \tag{2}$$

The source term S_{Latent} in Eq. 2 accounts for the evolution of the latent heat during phase change. The source term Q_{Losses} in Eq. 2 represents evaporation heat loss, radiation heat loss and convective heat loss due to the flowing argon gas. It is defined as

$$Q_{Losses} = \left(q''_{evaporation} + q''_{radiation} + q''_{conv}\right)|\nabla \gamma| \frac{2\rho C_{peff}}{\rho_{metal} C_{pmetal} + \rho_{gas} C_{pgas}} \tag{3}$$

The evaporation heat loss is the product of the latent heat of vaporization L_v and the vaporized mass flow rate $\dot{m}_v$.

$$q''_{evaporation} = -L_v \dot{m}_v \tag{4}$$

The vaporized mass flow rate of the escaping vapor $\dot{m}_v$ is given by:

$$\dot{m}_v = (1-\beta)\frac{M P_v}{\sqrt{2\pi M R T}} \tag{5}$$

where *M* is the molar mass, R is the ideal gas constant and P_v is the recoil vapor pressure which is given by

$$P_v = 0.54 P_0 exp\left[\frac{L_v M(T - T_v)}{RTT_v}\right] \quad (6)$$

where P_0 is the atmospheric pressure, L_v is the latent heat of vaporization and T_v is the vaporization temperature. β in Eq. 5 is the retro diffusion coefficient and it represents the extent of condensation of escaping vapour. In this study, $\beta = 0.18$ was assumed (Aggarwal et al., 2019). The source term Q_{Laser} in Eq. 2 accounts for heating by the moving laser beam. The energy input from the laser beam is approximated by a Gaussian distribution and is defined as

$$Q_{Laser} = \frac{2\eta P}{\pi {R_{spot}}^2} |\nabla \gamma| \frac{2\rho C_{peff}}{\rho_{metal} C_{pmetal} + \rho_{gas} C_{pgas}} \quad (7)$$

where η is the absorption coefficient.

The momentum conservation equation is given by

$$\frac{\partial(\rho \vec{U})}{\partial t} + \vec{U} \cdot \nabla(\rho \vec{U}) = -\nabla p + \nabla \cdot (\mu \left(\nabla \vec{U} + \left(\nabla \vec{U}\right)^T \right) + \overrightarrow{F_N} + \overrightarrow{F_D} + \overrightarrow{F_S} \quad (8)$$

The buoyant force due to the natural convection is implemented in the current model with the help of a source term $\overrightarrow{F_N}$ in Eq. (8) which is given as

$$\overrightarrow{F_N} = \rho_l \vec{g} \beta_T (T - T_{ref}) \quad (9)$$

where ρ_l, β_T and T_{ref} are the liquid metal density, thermal expansion coefficient and reference temperature, respectively. The source term $\overrightarrow{F_D}$ appearing in Eq. (8) is defined in Eq. (10). It aids to smoothly bring down the velocity of the fluid at the liquid-solid interface and makes the fluid velocity in the un-melted solid zone as zero.

$$\overrightarrow{F_D} = \frac{\left(1 - f_{liquid,metal}\right)^2}{{f_{liquid,metal}}^3 + b} C \vec{U} \quad (10)$$

The constant *C* in Eq. (10) represents mushy zone constant and a value of 160,000 kg m^{-3} s^{-1} is considered in the current model (Aggarwal et al., 2019). The term *b* is another constant having a small value (~10^{-6}) and is used to prevent division by zero when the liquid fraction ($f_{liquid,metal}$) becomes zero. The source term $\overrightarrow{F_S}$ in Eq. 8 term represents the forces which are acting at the interface and is given by

$$\overrightarrow{F_S} = \left\{\sigma \kappa \hat{n} + \frac{d\sigma}{dT}[\nabla T - \hat{n}(\hat{n} \cdot \nabla T)] + \hat{n}(P_v)\right\} |\nabla \gamma| \frac{2\rho}{\rho_m + \rho_g} \quad (11)$$

where σ is the surface tension coefficient, $\kappa = -(\nabla \cdot \hat{n})$ is the mean curvature of free surface, $\hat{n} = \nabla\gamma/|\nabla\gamma|$ is the interface normal unit vector and $d\sigma/dT$ is the temperature coefficient of surface tension. The first term represents the normal surface tension force, the second term represents the thermo-capillary force acting tangentially at the interface and the third term is the recoil pressure exerted by the metal vapour.

For thermo-fluidic particle scale modelling, a cell size of 10 µm provides grid independent and computationally efficient result. To make sure the solution is stable, self-adaptive time step based on the Courant Friedrichs Lewy condition was implemented. For each time step, phase fraction, mass conservation, Navier-Stokes, and thermal transport equations were solved.

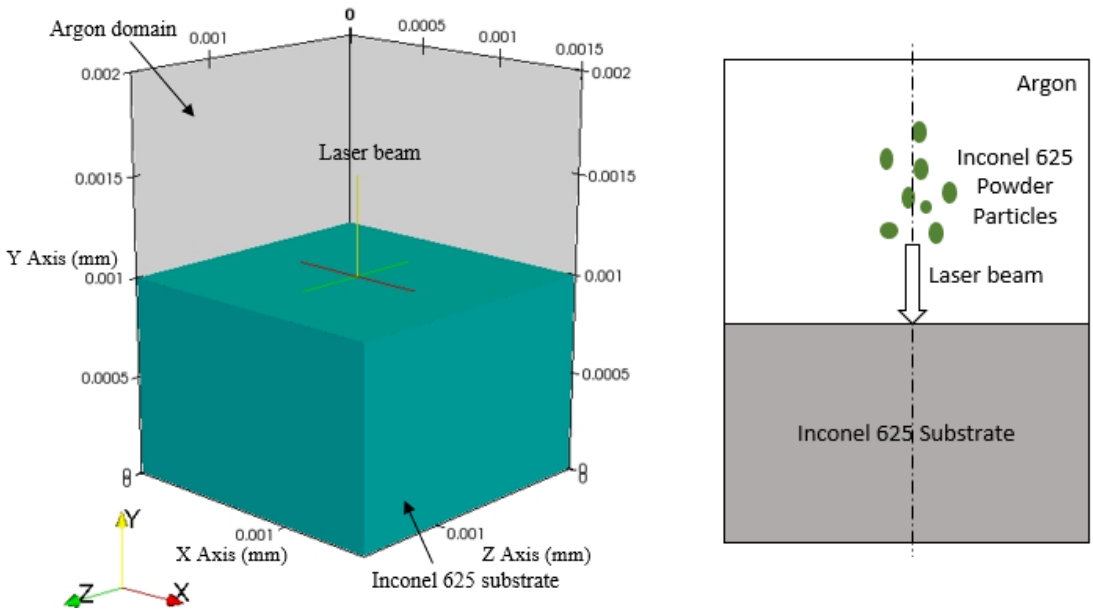

(a) (b)

Fig. 1. (a) Computational domain used for CFD simulation (b) Powder particle insertion

3. MATERIAL, METHODS AND EXPERIMENTS

In order to validate the simulation results and to obtain better understanding, single spots were deposited on an Inconel 625 substrate by varying the laser power and keeping all other process parameters the same (as given in Table 1). The spot deposition experiments were carried out using a laser-based LMD system (DMD 105D, POM). The LMD system consists of a diode laser of 1 kW power with a beam diameter of 0.3 mm. The single spots were deposited on a 10 mm thick Inconel 625 substrate. The deposited single spots were cross-sectioned at a center plane and then polished following standard metallographic procedures. To reveal the melt pool boundary and solidification microstructure, the polished samples were etched with HCl: H2O:HNO3 (1:1:1) solution. Microstructural characterization was carried out using an optical microscopy and a FESEM.

Table 1. Process parameters used in experiments

Parameter	Value
Laser spot diameter (µm)	300
Inconel 625 powder flow rate (g/min)	4
Laser on time (ms)	100
Laser power (W)	200, 400
Inconel 625 sheet thickness (mm)	10

4. Results and discussion

Spot laser metal deposition has been simulated for two beam power (P = 200 W and P = 400 W) keeping all other process parameters to be the same. Fig. 2 shows the temperature plot of the deposited single spot at different times for P = 200 W. In the figure the substrate, the melt pool and the powder particle stream can be clearly seen. Due to heating by the laser beam the powder particles and substrate melts and forms a bulk melt. Once the laser beam is off, the bulk melt re-solidified into bulk solid.

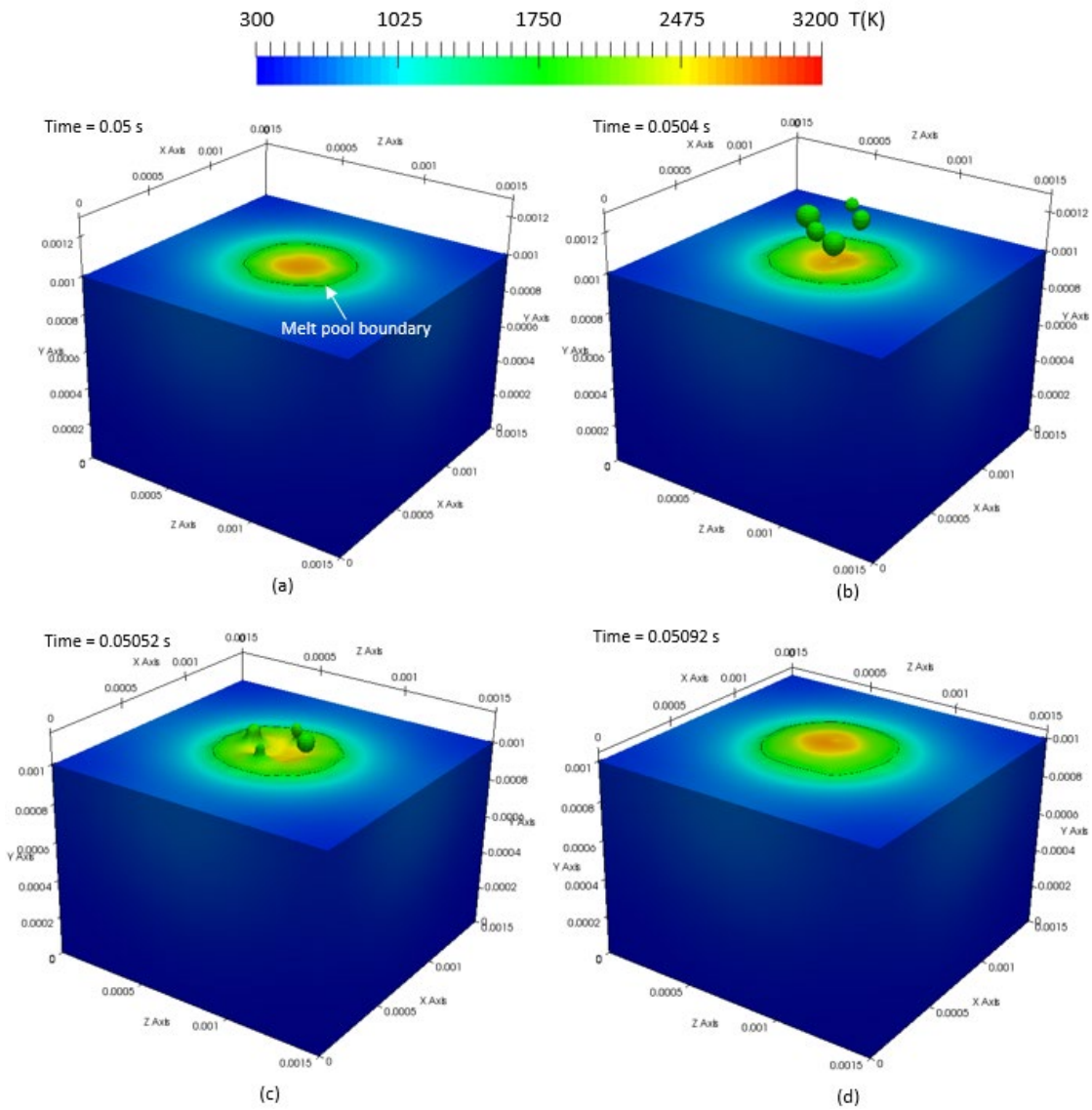

Fig. 2. Simulation results (P = 200 W) showing the melt pool formation and particle impingement during LMD process (a) Initial substrate heating, (b) Particles insertion, (c) Particles impingement, (d) Final stage

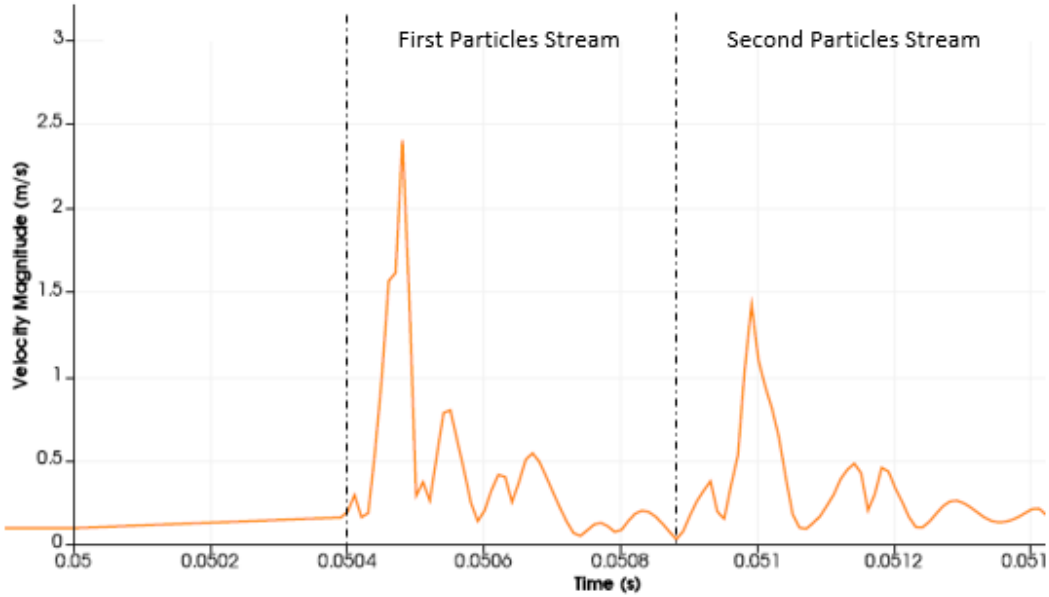

Fig. 3. Simulations result of the velocity magnitude variation with time at the center point of the computational domain showing the oscillatory behavior during the particle impingement stage (P = 200 W)

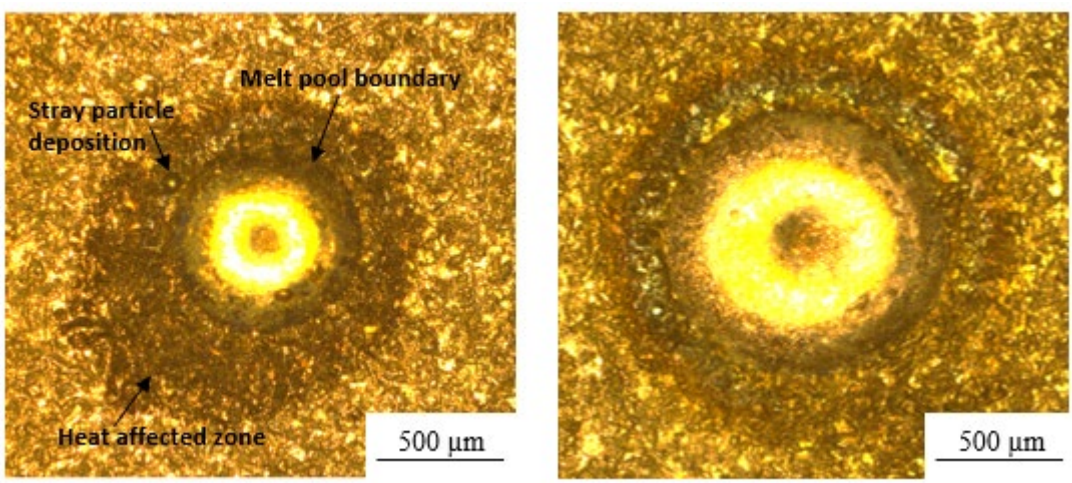

Fig. 4. Optical micrograph of the deposited single spot (top view), (a) Power = 200 W (b) Power = 400 W

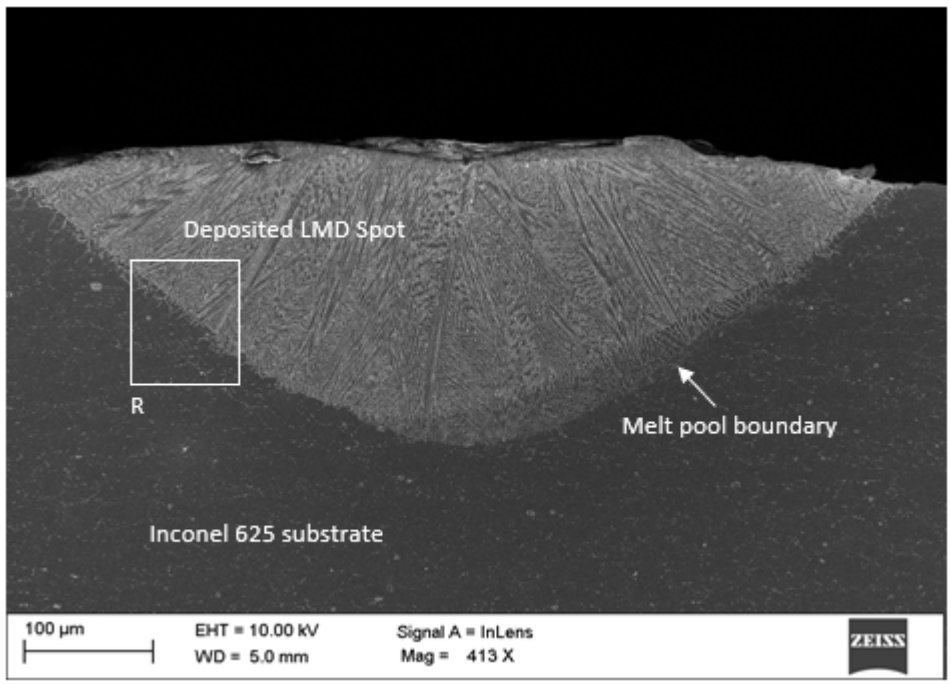

(a)

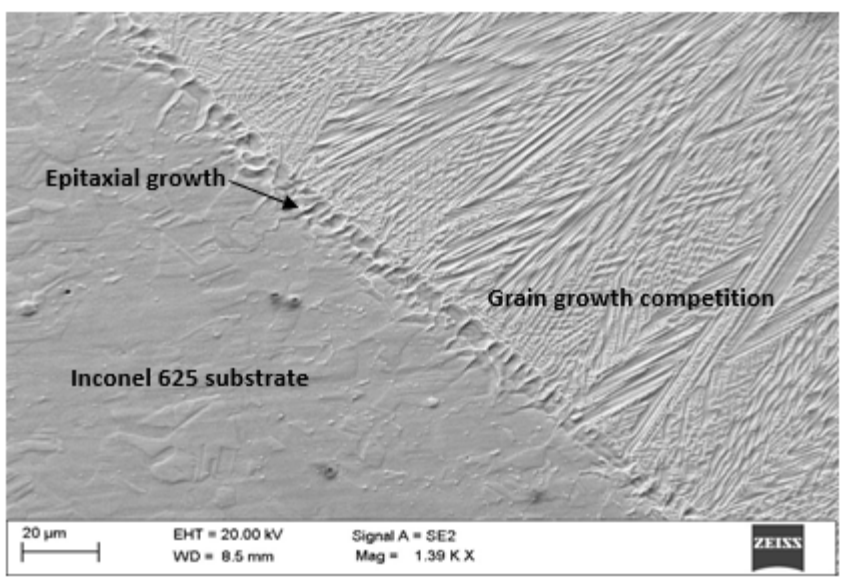

(b)

Fig. 5. (a) FE-SEM micrographs displaying melt pool boundaries and microstructure of single spot deposition (b) Magnified micrograph of region R in (a).

Figure 3 shows plot of velocity magnitude with time at the centre point of the computational domain for the laser power, P = 200 W, illustrating the melt pool instabilities. It can be clearly seen that as the powder particles impinges the melt pool, velocity magnitude starts fluctuating and generates oscillatory flow inside the melt pool. At time, t = 0.0504 s, the first stream of powder particles hit the melt pool, as a result velocity magnitude fluctuates from 2.4 m/s to 0.1 m/s. Subsequently, another powder stream hit the melt pool generating the same effect. These instabilities helps in redistributing the hot molten metal from the centre of the molten pool to its periphery. Therefore, maximum temperature of the molten pool drops significantly.

In order to quantitatively validate the simulation results and to obtain better understanding of the melt pool microstructure, single spots were deposited by varying the laser power. The spots were deposited on a 10 mm thick Inconel 625 substrate with a powder mass flow rate of 4 g/min. Figure 4 shows the top view of the deposited single spots at P = 200 W and P = 400 W. Fig. 5a and 5b shows the SEM micrograph, as shown, at first, there was epitaxial grain growth, then favourable dendrites along the maximum heat flux direction grows fastest, i.e., perpendicular to the melt pool interface. The simulated melt pool depth (198 µm) has a good agreement with the experimentally determined depth (203.1 µm). The simulated substrate melting width (610 µm) is slightly lower than the experimentally determined width (663.57 µm). The possible reasons for the slight under-prediction of the substrate melting width can be because of the consideration of temperature independent thermophysical properties of the Inconel 625 in the simulations.

4. Conclusions

3D particle scale thermo-fluidic modelling is performed to study the transport phenomena (convection, melting/ solidification phase change and instability formation) in the Laser Metal Deposition (LMD) process. The simulated melt pool characteristic dimensions matches well with the experimental data on melt pool dimensions. It was found that the high velocity impinging powder particles substantially influences the transport phenomena (velocity and temperature) in the melt pool causing instabilities. These instabilities generates circulatory flow inside the melt pool leading to a significant drop in the maximum temperature and velocity. The solidification microstructure shows that grain grows by epitaxial growth on the partially melted grain followed by a competitive grain growth.

Acknowledgements

The authors are highly thankful to Mr. Manjunath BN (Department of Ultra Precision Engineering, Central Manufacturing Technology Institute, Bengaluru, India) for his help in carrying out the experiments.

References

Aggarwal, A., Patel, S., Kumar, A., 2019. Selective Laser Melting of 316L Stainless Steel: Physics of Melting Mode Transition and Its Influence on Microstructural and Mechanical Behavior. JOM, 71(3), pp.1105-1116.

Kumar, A., Roy, S., 2009. Effect of three-dimensional melt pool convection on process characteristics during laser cladding. Computational Materials Science, 46(2), pp.495-506.

Lee, Y.S., Farson, D.F., 2016. Surface tension-powered build dimension control in laser additive manufacturing process. The International Journal of Advanced Manufacturing Technology, 85(5-8), pp.1035-1044.

Lee, Y.S., Nordin, M., Babu, S.S., Farson, D.F., 2014. Influence of fluid convection on weld pool formation in laser cladding. Welding Journal, 93(8), pp.292S-300S.

Manvatkar, V., De, A., DebRoy, T., 2014. Heat transfer and material flow during laser assisted multi-layer additive manufacturing. Journal of Applied Physics, 116(12), p.124905.